

MAJOR PAPER

Evaluating the Effect of Arterial Pulsation on Cerebrospinal Fluid Motion in the Sylvian Fissure of Patients with Middle Cerebral Artery Occlusion Using Low b-value Diffusion-weighted Imaging

Toshiaki Taoka^{1,2*}, Hisashi Kawai², Toshiki Nakane², Takashi Abe²,
Rei Nakamichi², Rintaro Ito^{1,2}, Yutaro Sasaki², Ayumi Nishida²,
and Shinji Naganawa²

Purpose: Decrease in signal of the cerebrospinal fluid (CSF) on low b-value diffusion weighted image (DWI) due to non-uniform flow can provide additional information regarding CSF motion. The purpose of the current study was to evaluate whether arterial pulsations constitute the driving force of CSF motion.

Methods: We evaluated the CSF signals within the Sylvian fissure on low b-value DWI in 19 patients with unilateral middle cerebral artery (MCA) occlusion. DWI with b-value of 500 s/mm² was evaluated for a decrease in CSF signal within the Sylvian fissure including the Sylvian vallicula and lower, middle, and higher Sylvian fissures and graded as follows: the same as contralateral side; smaller signal decrease than that on contralateral side; and no signal decrease. MR angiography (MRA) findings of MCA were graded as follows: the same as contralateral, lower signal than contralateral signal, and no signal. In 15 patients, regional cerebral blood flow (rCBF) was evaluated using single-photon emission computed tomography (SPECT) studies and graded as > 90%, 90%–70%, and < 70% rCBF compared to contralateral. The correlations between the gradings were evaluated using G likelihood-ratio test.

Results: There was no statistically significant correlation between the MRA and low b-value DWI gradings of CSF in all areas. There were statistically significant correlations between the decreases in CBF on SPECT and CSF signals in the middle Sylvian fissure.

Conclusion: The driving force of CSF pulsation in the Sylvian sinus may be related to the pulsations of the cerebral hemisphere rather than direct arterial pulsations.

Keywords: cerebrospinal fluid motion, diffusion-weighted imaging, low b-value, cerebral artery occlusion

Introduction

Since the introduction of the Glymphatic system by Iliff et al.,¹ several studies have been published on the dynamics between cerebrospinal fluid (CSF) and interstitial fluid (ISF).^{2–16} However, there are several unsolved questions about the

dynamics between CSF and ISF; one of them is the mechanism behind the pulsatile motion of CSF. Multiple studies have been published on the CSF dynamics within the brain parenchyma.^{17,18} Iliff et al. used *in vivo* two-photon microscopy in mice to visualize vascular wall pulsatility in intracortical arteries; they found that unilateral ligation of the internal carotid artery significantly reduced arterial pulsatility. They concluded that cerebral arterial pulsatility is a key driver of perivascular CSF influx into the brain parenchyma.¹⁷ Mestre et al. used particle tracking velocimetry in live mice and reported that the speed of the arterial wall matches that of CSF, thus suggesting that arterial wall motion is the principal driving mechanism of CSF in the perivascular space.¹⁸

The pulsatile motion of the CSF within the subarachnoid space has also been studied. The time-spatial inversion pulse (time-SLIP) method and the phase contrast (PC) method have been applied to evaluate and visualize the CSF motion in the brain and ventricles.^{19–21} One of the findings of a previous study has cast doubt on arterial pulsation in the

¹Department of Innovative Biomedical Visualization (iBMV), Nagoya University Graduate School of Medicine, Nagoya, Aichi, Japan

²Department of Radiology, Nagoya University Graduate School of Medicine, Nagoya, Aichi, Japan

*Corresponding author: Department of Innovative Biomedical Visualization (iBMV), Nagoya University Graduate School of Medicine, 65, Tsurumaicho, Showa-ku, Nagoya, Aichi 466-8550, Japan. Phone: +81-52-744-2328, Fax: +81-52-744-2335, E-mail: ttaoka@med.nagoya-u.ac.jp



This work is licensed under a Creative Commons Attribution-NonCommercial-NoDerivatives International License.

©2021 Japanese Society for Magnetic Resonance in Medicine

Received: August 26, 2020 | Accepted: October 14, 2020

choroid plexus being the driving force of CSF motion.²⁰ In addition to the aforementioned methods, a decrease in signal on low b-value diffusion weighted imaging (DWI) can also be applied to evaluate the CSF dynamics within the subarachnoid space of the brain and ventricles.^{16,22} A study that used low b-value DWI demonstrated that relatively large arteries tended to be conspicuous in some CSF spaces, such as the Sylvian fissure or ambient cistern,¹⁶ which further questions whether arterial pulsation is the driving force for CSF pulsation within the Sylvian fissure. If arterial pulsation is the direct driving force for CSF pulsation, then CSF pulsation within the Sylvian fissure on an obstruction side may become weak in cases of horizontal occlusion of the middle cerebral artery (MCA).

We hypothesized that the decrease in signal within the Sylvian fissure on low b-value DWI would be smaller on the side of MCA occlusion or severe stenosis. The aim of this study was to evaluate the decrease in signal within the Sylvian fissure on low b-value DWI in unilateral MCA occlusion or severe stenosis and compare that with the signal on time-of-flight (TOF) MR angiography (MRA) and regional cerebral blood flow (rCBF).

Materials and Methods

Patients

This retrospective study was approved by the institutional review board of our institute. The patients were retrospectively enrolled from the image server of our institute; they underwent imaging with a single 3.0-T clinical scanner (Magnetom Skyra; Siemens, Munich, Germany) with a fixed DWI sequence. For inclusion in the study, we performed a text search on the image report server “Skyra” as the scanner, “DWI” as the method, and “middle cerebral artery” and “occlusion” as keywords for the diagnosis between January 2012 and July 2020. Of the images of 41 patients that fulfilled the criteria, we excluded those with duplication using follow-up studies (n = 6), bilateral occlusion (n = 6), hemorrhage (n = 5), post-aneurysm surgery (n = 3), and occlusion not in the horizontal portion but peripheral to MCA bifurcation (n = 2). Consequently, 19 patients (age, 19–84 years; 12 males) were included in the evaluation. The underlying disorder of MCA occlusion was moyamoya disease in 7 patients and arteriosclerosis in 12 patients. CBF was evaluated in 15 of these patients. The MCA occlusion sides were left in 10 patients and right in 9 patients.

Imaging

MR images that were retrospectively evaluated in the current study were scanned using a 3.0-T clinical scanner. Since the patients were enrolled from routine clinical studies, the images were obtained using the usual clinical protocols and DWIs. The parameters for DWI were as follows: TR = 5000 ms; TE = 85 ms; EPI factor = 192; Echo spacing = 1.04 ms; Bandwidth

= 1086 Hz/Px; FOV = 220 mm; 192 × 192, 25 slices with distant factor = 20%; slice thickness = 5 mm; averages = 1; acceleration factor = 2; acquisition time = 1 min 22 s; motion proving gradient: bipolar type, b-value = 0, 500, 1000 s/mm²; 3-scan trace; fat suppression; and no flow compensation.

CBF was examined using the single-photon emission computed tomography (SPECT)/CT system (Symbia T; Siemens) with intravenously injected ¹²³I iodoamphetamine (167 MBq) and analyzed using 3D stereotaxic ROI template analysis²³ or 3D stereotactic surface projection (3D-SSP) analysis.^{24–26} 3D-SSP analysis provides a mean value of CBF in the brain areas of those supplied by the anterior cerebral artery, MCA, posterior cerebral artery, basal ganglionic region, thalamus, pons, cerebellar hemisphere, and cerebellar vermis.

Image analysis

All images were interpreted by consensus between two neurologists (SN and TT). We evaluated the signal intensity of CSF within the Sylvian fissure using low b-value DWI with b = 500 s/mm². Evaluations were performed in four slice positions at the levels of the Sylvian vallecule, lower Sylvian fissure, middle Sylvian fissure, and upper Sylvian fissure (Figs. 1 and 2).

The signal intensity of CSF within the Sylvian fissure on the affected side on low b-value DWI was evaluated qualitatively and compared with that on the unaffected contralateral Sylvian fissure within the same imaging slices. A decrease in signal equal to that on the unaffected side, a decrease in signal smaller than that on the unaffected side, and no decrease in signal were graded as A, B, and C, respectively.

The signal intensity of MCA on the affected side on TOF-MRA was also evaluated qualitatively and graded. No arterial signal, lower arterial signal than that on the unaffected side, and arterial signal equal to that on the unaffected side were graded as I, II, and III, respectively.

CBF was evaluated using the results of 3D-SSP analysis. Ratio of the rCBF of the MCA territory on the affected side and that on the unaffected side was calculated; the ratio of > 90%, 90%–70%, and < 70% were graded as I, II, and III, respectively.

G likelihood-ratio test was used to compare the decrease in the CSF signal within the Sylvian fissure on low b-value DWI and that of MCA on TOF-MRA. The test was also used to compare the decrease in the CSF signal within the Sylvian fissure on low b-value DWI and CBF of the MCA territory.

Results

On low b-value DWI, areas of a decrease in signal in the Sylvian vallecule were smaller on the side of MCA occlusions in 11 patients, while they were equal to those on the unaffected side in the remaining eight patients. In the lower Sylvian fissure, no signal decrease on the side of MCA occlusion was observed in six patients; a signal decrease smaller than

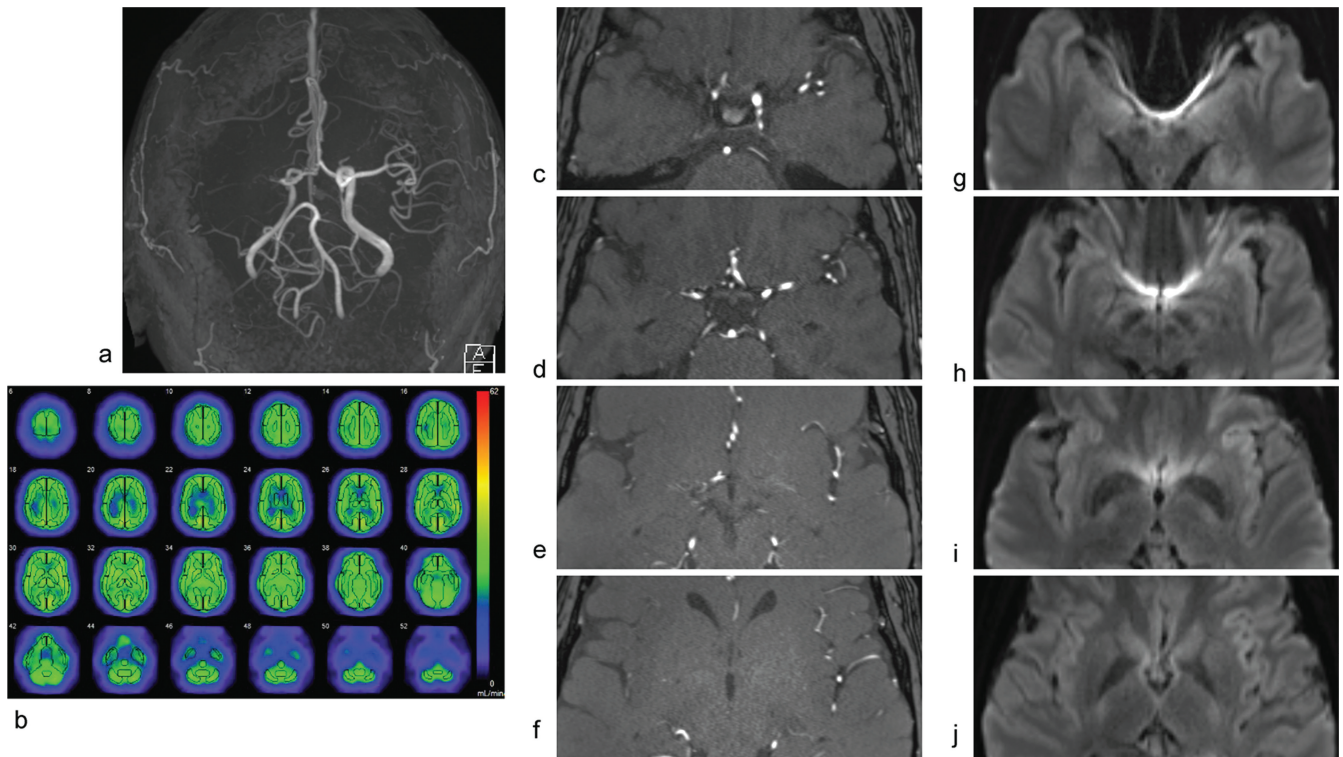


Fig. 1 A 45-year-old patient with moyamoya disease with occlusion of the origin of the right MCA. (a) TOF-MRA (maximum intensity projection); (b) ^{123}I iodoamphetamine SPECT using 3D stereotactic surface projection analysis; (c–f) TOF-MRA (source image); (g–j) low b-value DWI. TOF-MRA (a and c) revealed occlusion of the horizontal portion of MCA and small collateral arteries. Visualization of the peripheral branches of MCA was poor (d–f). SPECT (b) revealed a small decrease in rCBF in the right MCA territory (96% to the right MCA territory). On low b-value DWI, the signal decrease was equal to that on the unaffected side in all areas including the Sylvian vallicula (g) and lower (h), middle (i), and upper Sylvian fissure (j). CBF, cerebral blood flow; DWI, diffusion weighted image; MCA, middle cerebral artery; MRA, magnetic resonance angiography; SPECT, single-photon emission computed tomography; TOF, time-of-flight.

that on the unaffected side was observed in six patients; and signal decrease equal to that on the unaffected side was observed in seven patients. In the middle Sylvian fissure, similar findings were observed in seven, six, and six patients, respectively. In the upper Sylvian fissure, a signal decrease on the side of MCA occlusion smaller than that on the unaffected side was observed in 6 patients and a signal decrease equal to that on the unaffected side was observed in 13 patients. Representative images are presented in Figs. 1 and 2.

Comparisons between the decrease in the CSF signal on low b-value DWI within the Sylvian fissure and the signal on TOF image are presented in Fig. 3. There were no statistically significant correlations between the signal decrease on low b-value DWI and the arterial signal on TOF in any part of the Sylvian fissure. In the analysis of all areas within the Sylvian fissure, there were no statistically significant correlations.

Comparisons between the decrease in CSF signal on low b-value DWI within the Sylvian fissure and rCBF of the MCA territory are presented in Fig. 4; a statistically significant correlation was observed between them ($P = 0.018$). In the analysis of all areas within the Sylvian fissure, the

decrease in signal on low b-value DWI in the Sylvian fissure and rCBF were significantly correlated ($P = 0.001$).

Discussion

Evaluation of CSF dynamics using several non-invasive MRI techniques has been reported in humans. The time-SLIP method is a method in which a slab of an inversion pulse is applied to the CSF and its movements are visualized using the CSF itself as a tracer. Since no exogenous tracer is required in the time-SLIP method, CSF dynamics can be observed in natural physiological conditions.¹⁹ This method has demonstrated “to and fro” pulsations in the isthmus of the ventricular system, such as the foramen of Monro and the aqueduct. These movements are observed from the prepontine and basilar cisterns to the Sylvian fissure. However, neither continuous flow nor pulsation of the CSF is observed between the Sylvian fissure and cerebral fornix. The superficial Sylvian vein is present in this region and the arachnoid membrane that covers it is strongly adherent to the vein, which indicates that the Sylvian fissure is at the distal end of the subarachnoid space.²⁷ A PC method is a method for evaluating the phase shift

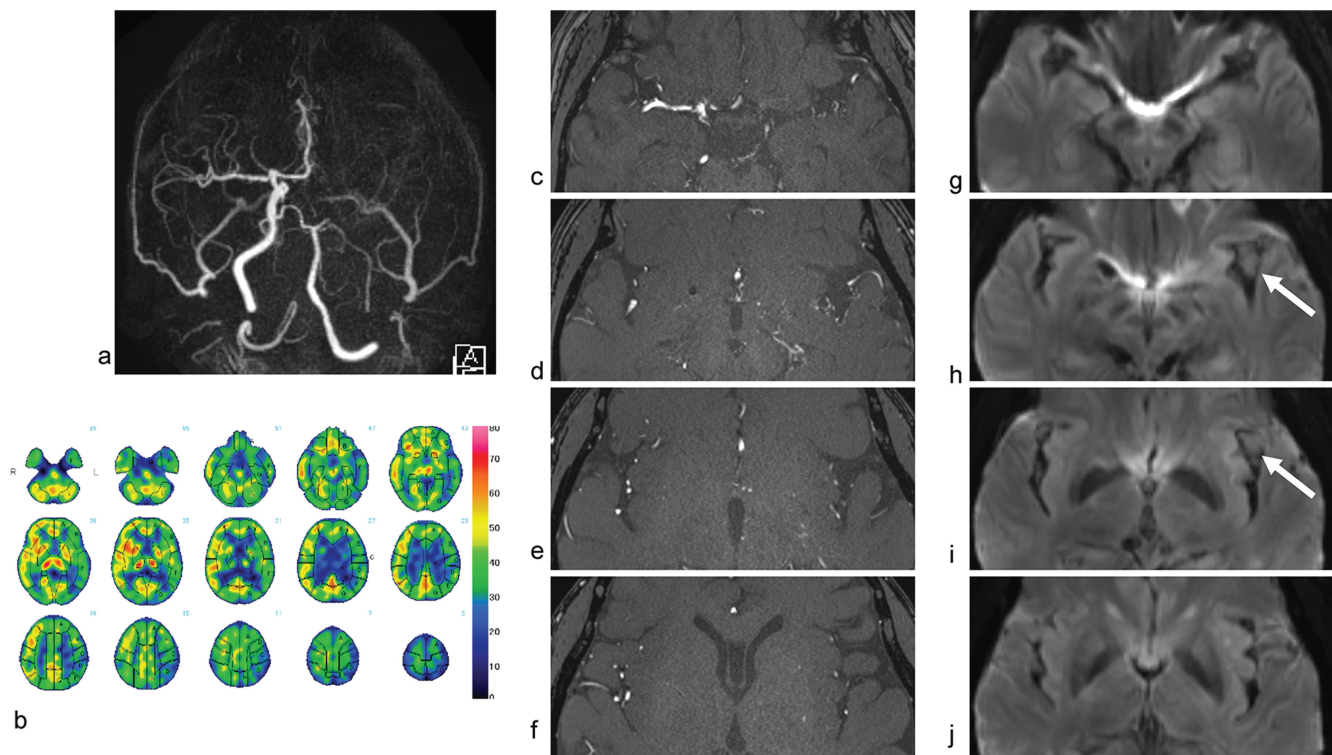


Fig. 2 A 63-year-old male with arteriosclerotic occlusion of the left internal carotid artery and left MCA. **(a)** TOF-MRA. (maximum intensity projection); **(b)** ^{123}I iodoamphetamine SPECT using 3D stereotaxic ROI template analysis; **(c–f)** TOF-MRA (source image); **(g–j)** low b-value DWI. TOF-MRA (**a** and **c**) demonstrated occlusion of the horizontal part of MCA and small collateral arteries. Peripheral branches of MCA are visualized (**d–f**). SPECT (**b**) revealed a decreased rCBF in the left MCA territory (78% to the right MCA territory). On low b-value DWI, signal decrease was equal to that on the unaffected side in the Sylvian vallicula (**g**) and upper Sylvian fissure (**j**), while in the lower and middle Sylvian fissures (**h** and **i**), the signal decrease was smaller than that on the unaffected side but a large part of the area revealed no signal decrease (arrows). CBF, cerebral blood flow; DWI, diffusion weighted image; MCA, middle cerebral artery; MRA, magnetic resonance angiography; SPECT, single-photon emission computed tomography; TOF, time-of-flight.

depending on the spin speed; it is another non-invasive method for observing CSF dynamics in humans. Recently, the 4D-PC method, which provides quantitative spatiotemporal velocity distribution, has also been applied to study CSF dynamics.²⁸ Similar findings regarding CSF dynamics as those with the time-SLIP method were observed using the 4D-PC method, including the pulsatile “to and fro” movements in the isthmus of the ventricular system and less movement of the CSF in the cranial vault. The 4D-PC study also demonstrated that CSF around the Sylvian sinus flows downward during cardiac systole and upward during diastole. It has been demonstrated that the movement of CSF is significantly modified not only by the cardiac pulse but also by respiration.²⁹

In 1986, Le Bihan et al. published a report on intravoxel incoherent motions (IVIMs), which resulted in the concepts of DWI and apparent diffusion coefficient (ADC).³⁰ In the report, they discussed that the non-uniform slow-flow effect of CSF according to the existence in a single voxel of several velocities results in echo attenuation of DWI and higher ADC. Furthermore, they discussed that this phenomenon may have a useful clinical application in IVIM or diffusion images.³⁰ The signal intensity on DWI depends

primarily on the relaxation time, proton density, intra-voxel diffusion, and perfusion; DWI enables visualization of the motion of water molecules as a decrease in signal due to phase shift created by the motion. When the phase shift becomes larger than $\pm\pi$ or when various velocities exist in a single voxel, the signal decrease on DWI becomes prominent depending on the b-values (motion-related signal dephasing). A study reported that a low b-value DWI of $b = 500 \text{ s/mm}^2$ reflected changes in the dynamics of CSF.¹⁶ The study reported that CSF within the lateral ventricle on low b-value DWI with $b = 500 \text{ s/mm}^2$ demonstrated higher signals in the ventricle dilatation group than in the control group. Moving protons, such as those found in CSF, result in a decrease in signal on DWI, which is greater when the flow is faster or b-value is larger. When the motion-probing gradient (MPG) of $b = 1000 \text{ s/mm}^2$ is used, the signal intensity of CSF on DWI is suppressed significantly anywhere in CSF. However, when MPG is lower, such as $b = 500 \text{ s/mm}^2$, the CSF signal is not suppressed completely, particularly in the portion of the signal from static protons in CSF, which is the basis of the “T2 shine through” phenomenon. Therefore, the finding that the

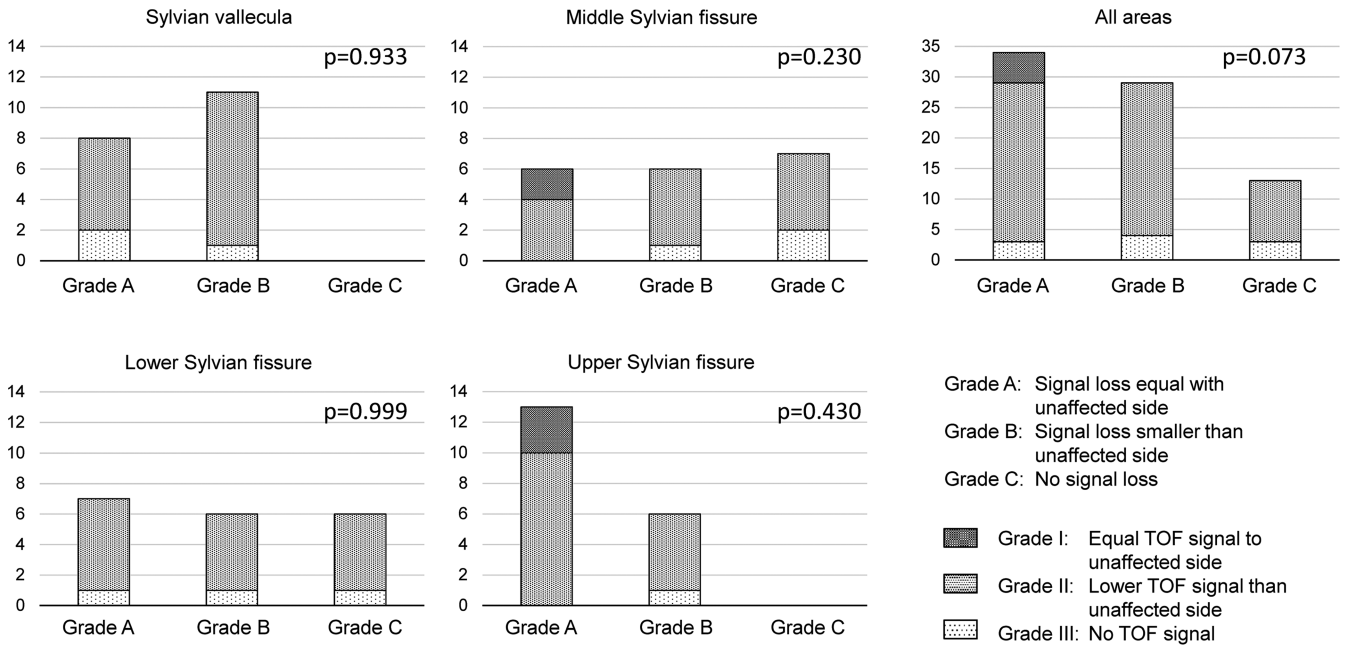


Fig. 3 Comparisons between the CSF signal decrease on DWI using $b = 500 \text{ s/mm}^2$ within the Sylvian fissure and the signal on TOF image. There were no statistically significant correlations on G likelihood-ratio test between the signal decrease on low b-value DWI and the arterial signal on TOF in any part of the Sylvian fissure. CSF, cerebrospinal fluid; DWI, diffusion weighted image; TOF, time-of-flight.

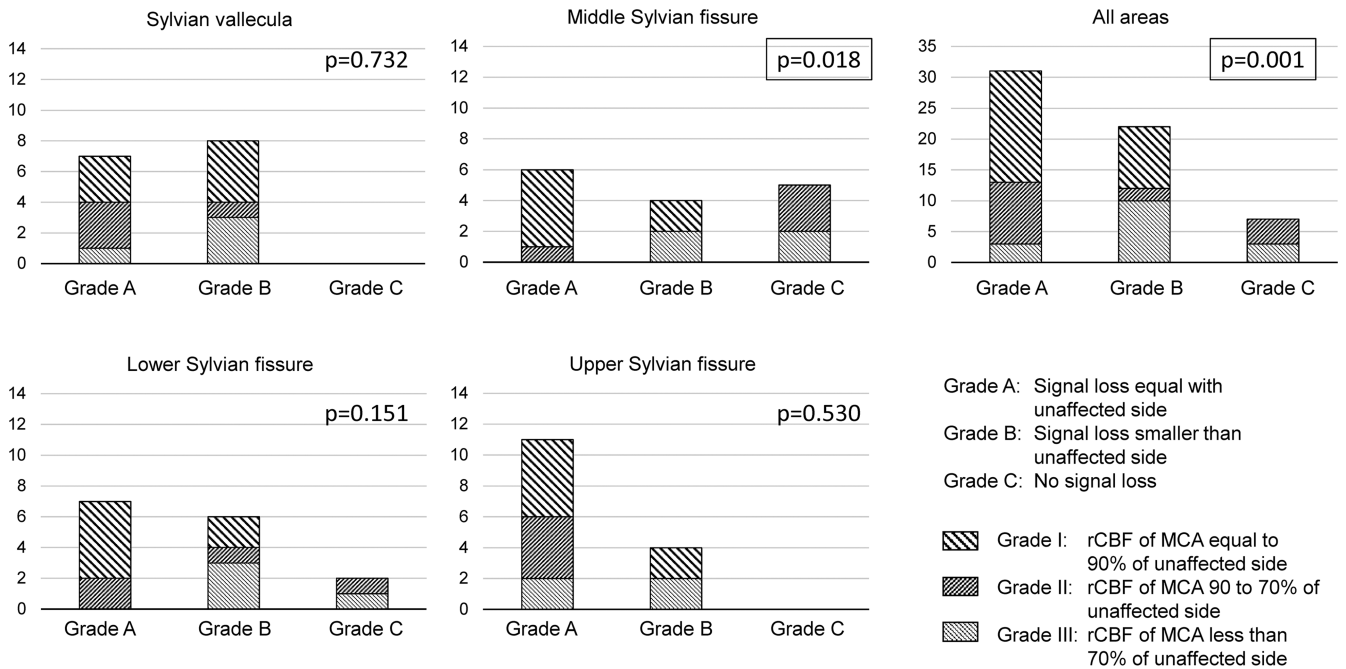


Fig. 4 Comparisons between the decrease in CSF signal on DWI with $b = 500 \text{ s/mm}^2$ within the Sylvian fissure and the rCBF of the MCA territory. There was a statistically significant correlation between the signal decrease on low b-value DWI in the middle Sylvian fissure and rCBF ($P = 0.018$). In the analysis of all areas within the Sylvian fissure, there was statistically significant correlation between the signal decrease on low b-value DWI in the Sylvian fissure and rCBF ($P = 0.001$). CSF, cerebrospinal fluid; DWI, diffusion weighted image; MCA, middle cerebral artery; rCBF, regional cerebral blood flow.

CSF signal intensity within the ventricle was higher in the cases of ventricular dilatation implies that the motion of the water molecules is slower compared to that in controls.

Several studies have evaluated CSF dynamics using low b-value diffusion imaging, such as the diffusion tensor method²² or use of multiple b-values.³¹

A previous study on CSF signal on low b-value DWI reported that the signal decrease tended to be conspicuous in locations of relatively large arteries, such as the Sylvian fissure and prepontine cistern,¹⁶ which suggests that the driving force of CSF dynamics may be the pulsations of these large arteries. This finding was the motivation for the current study to evaluate the effects of the pulsations of large arteries on CSF dynamics; we hypothesized that the signal decrease within the Sylvian fissure on low b-value DWI would be smaller on the side of MCA occlusion or severe stenosis. However, the results of the current study revealed those were not significant correlations between the MCA signal on TOF-MRA and the grades for decrease in CSF signal on low b-value DWI at any site, including the Sylvian vallecule and Sylvian fissure. In contrast, in the middle part of the Sylvian fissure, a statistically significant correlation was observed between the decrease in rCBF in the MCA territory on SPECT and the decrease in CSF signal on low b-value DWI. Additionally, a statistically significant correlation was observed when the entire Sylvian vallecule and fissure was evaluated. It is considered that this is because the number of samples was increased by collecting the observation points of the Sylvian fissure, which was statistically advantageous. Since the laterality of the MCA occlusion in the current population is almost equal, laterality might not be a confounder. These results may indicate that the direct arterial pulsations may only be a part of the driving force within the Sylvian vallecule and Sylvian fissure; however, their effects on CSF dynamics are limited. We believe that indirect pulsations due to the pulsations of the cerebral parenchyma, which is represented by CBF, have comparative effects on CSF dynamics within the Sylvian vallecule and fissure. Additionally, the effects would be larger from physiological motion, such as the motion of the brain during respiration, than from cardiac pulsations. There are previous reports to suggest that the respiratory motion has a large influence to the CSF dynamics by indicating contribution of respiration on CSF velocity in the aqueduct or foramen magnum.^{32,33}

This study has several limitations. The first limitation in the current study is that the evaluation was made qualitatively by scoring methods. One of the reasons is the complexity in the morphological shape of the CSF space within the cranium. Signal or ADC quantification by placing manual ROI in such condition would be suffered by the bias, and quantification by using a mask would suffer from contamination from adjacent structures. We selected qualitative evaluation by scoring methods in order to avoid incomplete signal or ADC quantification. We evaluated the TOF signal of MCA also qualitatively by scores. This is because the TOF signal intensity might not directly reflect the intensity of arterial pulsation. We evaluated the TOF signal as a descriptor of the MCA stenosis or occlusion. The second limitation is the study was designed as a retrospective study using clinically obtained images. The number of the patients is small because we tried to evaluate the images using the identical image acquisition protocol.

Patient selection in the current study was based on the description of clinical reports and not optimally randomized ones; therefore, not all the included patients had rCBF images using SPECT. The third limitation is the lack of optimization of the sequence, especially in the b-value. The single b-value of 500 s/mm² may not be optimal for the evaluation of CSF dynamics but is optimal for the calculation of ADC values in daily clinical practice. DWI by various b-values can visualize the degree of the CSF motion. DWI with lower b-value will show motion-related signal dephasing only in the area with larger CSF motion, while DWI with higher b-value will show motion-related signal dephasing of the CSF in wide area with small to large CSF motion.

Conclusion

We investigated the decrease in CSF signal in the Sylvian vallecule and fissure in patients with MCA occlusion using DWI with b-value of 500 s/mm². No statistical correlation was observed between the visualization of MCA on MRA and the degree of the decrease in CSF signal on low b-value DWI at any site. A statistically significant correlation was observed between the decrease in rCBF in the MCA territory and the degree of the decrease in CSF signal on low b-value DWI in the Sylvian fissure. The driving force of CSF pulsation in the Sylvian sinus may be related to the pulsations of the cerebral hemisphere rather than direct arterial pulsations.

Conflicts of Interest

The Department of Innovative Biomedical Visualization (iBMV), Nagoya University Graduate School of Medicine is financially supported by Canon Medical Systems Corporation.

References

1. Iliff JJ, Wang M, Liao Y, et al. A paravascular pathway facilitates CSF flow through the brain parenchyma and the clearance of interstitial solutes, including amyloid β . *Sci Transl Med* 2012; 4:147ra111.
2. Naganawa S, Ito R, Kawai H, et al. Confirmation of age-dependence in the leakage of contrast medium around the cortical veins into cerebrospinal fluid after intravenous administration of gadolinium-based contrast agent. *Magn Reson Med Sci* 2020; 19:375–381.
3. Naganawa S, Ito R, Nakamichi R, et al. Relationship between parasagittal perivenous cysts and leakage of gadolinium-based contrast agents into the subarachnoid space around the cortical veins after intravenous administration. *Magn Reson Med Sci* 2021; 20:245–252.
4. Naganawa S, Ito R, Taoka T, et al. The space between the pial sheath and the cortical venous wall may connect to the meningeal lymphatics. *Magn Reson Med Sci* 2019; 19:1–4.
5. Naganawa S, Nakane T, Kawai H, et al. Gd-based contrast enhancement of the perivascular spaces in the Basal Ganglia. *Magn Reson Med Sci* 2017; 16:61–65.

6. Naganawa S, Nakane T, Kawai H, et al. Lack of contrast enhancement in a giant perivascular space of the basal ganglion on delayed FLAIR images: Implications for the glymphatic system. *Magn Reson Med Sci* 2017; 16:89–90.
7. Naganawa S, Nakane T, Kawai H, et al. Differences in signal intensity and enhancement on MR images of the perivascular spaces in the basal ganglia versus those in white matter. *Magn Reson Med Sci* 2018; 17:301–307.
8. Naganawa S, Nakane T, Kawai H, et al. Age dependence of gadolinium leakage from the cortical veins into the cerebrospinal fluid assessed with whole brain 3D-real inversion recovery MR imaging. *Magn Reson Med Sci* 2019; 18:163–169.
9. Naganawa S, Nakane T, Kawai H, et al. Detection of IV-gadolinium leakage from the cortical veins into the CSF using MR fingerprinting. *Magn Reson Med Sci* 2020; 19:141–146.
10. Taoka T, Jost G, Frenzel T, et al. Impact of the glymphatic system on the kinetic and distribution of gadodiamide in the rat brain: observations by dynamic MRI and effect of circadian rhythm on tissue gadolinium concentrations. *Invest Radiol* 2018; 53:529–534.
11. Taoka T, Masutani Y, Kawai H, et al. Evaluation of glymphatic system activity with the diffusion MR technique: diffusion tensor image analysis along the perivascular space (DTI-ALPS) in Alzheimer's disease cases. *Jpn J Radiol* 2017; 35:172–178.
12. Taoka T, Naganawa S. Gadolinium-based contrast media, cerebrospinal fluid and the glymphatic system: possible mechanisms for the deposition of gadolinium in the Brain. *Magn Reson Med Sci* 2018; 17:111–119.
13. Taoka T, Naganawa S. Glymphatic imaging using MRI. *J Magn Reson Imaging* 2020; 51:11–24.
14. Taoka T, Naganawa S. Neurofluid dynamics and the glymphatic system: a neuroimaging perspective. *Korean J Radiol* 2020; 21:1199–1209.
15. Taoka T, Naganawa S. Imaging for central nervous system (CNS) interstitial fluidopathy: disorders with impaired interstitial fluid dynamics. *Jpn J Radiol* 2021; 39:1–14.
16. Taoka T, Naganawa S, Kawai H, et al. Can low b value diffusion weighted imaging evaluate the character of cerebrospinal fluid dynamics? *Jpn J Radiol* 2019; 37:135–144.
17. Iliff JJ, Wang M, Zeppenfeld DM, et al. Cerebral arterial pulsation drives paravascular CSF-interstitial fluid exchange in the murine brain. *J Neurosci* 2013; 33:18190–18199.
18. Mestre H, Tithof J, Du T, et al. Flow of cerebrospinal fluid is driven by arterial pulsations and is reduced in hypertension. *Nat Commun* 2018; 9:4878.
19. Yamada S, Miyazaki M, Kanazawa H, et al. Visualization of cerebrospinal fluid movement with spin labeling at MR imaging: preliminary results in normal and pathophysiologic conditions. *Radiology* 2008; 249:644–652.
20. Takizawa K, Matsumae M, Hayashi N, et al. The choroid plexus of the lateral ventricle as the origin of CSF pulsation is questionable. *Neurol Med Chir (Tokyo)* 2018; 58:23–31.
21. Yatsushiro S, Sunohara S, Hayashi N, et al. Cardiac-driven pulsatile motion of intracranial cerebrospinal fluid visualized based on a correlation mapping technique. *Magn Reson Med Sci* 2018; 17:151–160.
22. Bito Y, Harada K, Ochi H, et al. Low b-value DTI for analyzing pseudo-random flow of CSF. Proceedings of the 28th Annual Meeting of ISMRM, Paris, France (WEB), 2020; 224.
23. Takeuchi R, Yonekura Y, Matsuda H, et al. Usefulness of a three-dimensional stereotaxic ROI template on anatomically standardised ^{99m}Tc-ECD SPET. *Eur J Nucl Med Mol Imaging* 2002; 29:331–341.
24. Minoshima S, Frey KA, Koeppe RA, et al. A diagnostic approach in Alzheimer's disease using three-dimensional stereotactic surface projections of fluorine-18-FDG PET. *J Nucl Med* 1995; 36:1238–1248.
25. Mizumura S, Nakagawara J, Takahashi M, et al. Three-dimensional display in staging hemodynamic brain ischemia for JET study: objective evaluation using SEE analysis and 3D-SSP display. *Ann Nucl Med* 2004; 18:13–21.
26. Yamauchi M, Imabayashi E, Matsuda H, et al. Quantitative assessment of rest and acetazolamide CBF using quantitative SPECT reconstruction and sequential administration of (123)I-iodoamphetamine: comparison among data acquired at three institutions. *Ann Nucl Med* 2014; 28:836–850.
27. Yamada S. Cerebrospinal fluid physiology: visualization of cerebrospinal fluid dynamics using the magnetic resonance imaging Time-Spatial Inversion Pulse method. *Croat Med J* 2014; 55:337–346.
28. Hirayama A, Matsumae M, Yatsushiro S, et al. Visualization of pulsatile CSF motion around membrane-like structures with both 4D velocity mapping and Time-SLIP technique. *Magn Reson Med Sci* 2015; 14:263–273.
29. Matsumae M, Kuroda K, Yatsushiro S, et al. Changing the currently held concept of cerebrospinal fluid dynamics based on shared findings of cerebrospinal fluid motion in the cranial cavity using various types of magnetic resonance imaging techniques. *Neurol Med Chir (Tokyo)* 2019; 59:133–146.
30. Le Bihan D, Breton E, Lallemand D, et al. MR imaging of intravoxel incoherent motions: application to diffusion and perfusion in neurologic disorders. *Radiology* 1986; 161:401–407.
31. Taoka T, Ito R, Nakamichi R, et al. Multi b-value Diffusion weighted image Diphase Map (MbDDM) to evaluate cerebrospinal fluid dynamics. Proceedings of the 28th Annual Meeting of ISMRM, Paris, France (WEB), 2020; 225.
32. Spijkerman JM, Geurts LJ, Siero JCW, et al. Phase contrast MRI measurements of net cerebrospinal fluid flow through the cerebral aqueduct are confounded by respiration. *J Magn Reson Imaging* 2019; 49:433–444.
33. Yildiz S, Thyagaraj S, Jin N, et al. Quantifying the influence of respiration and cardiac pulsations on cerebrospinal fluid dynamics using real-time phase-contrast MRI. *J Magn Reson Imaging* 2017; 46:431–439.